ACS OMEGA

Article

Cite This: ACS Omega 2019, 4, 19847−19855

http://pubs.acs.org/journal/acsodf

Fast Detection and Flexible Microfluidic pH Sensors Based on Al-Doped ZnO Nanosheets with a Novel Morphology

You-Ting Tsai,[†] Shoou-Jinn Chang,[†] Liang-Wen Ji,*[,‡] Yu-Jen Hsiao,[§] and I-Tseng Tang[∥]

[†]Institute of Microelectronics & Department of Electrical Engineering, Center for Micro/Nano Science and Technology, Advanced Optoelectronic Technology Center, National Cheng Kung University, Tainan 70101, Taiwan

[‡]Institute of Electro-Optical and Materials Science, National Formosa University, Yunlin 632, Taiwan

[§]Department of Mechanical Engineering, Southern Taiwan University of Science and Technology, Tainan 710, Taiwan

[∥]National University of Tainan, Department of Greenergy, Tainan 700, Taiwan

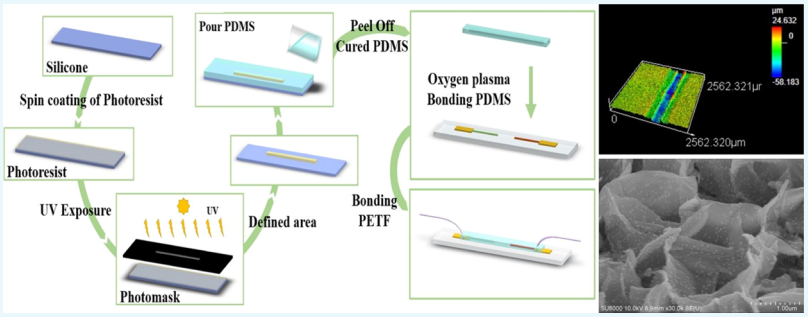

ABSTRACT: In this study, a flexible and stable pH sensor based on aluminum-doped zinc oxide nanosheets (Al-doped ZnO NSs) was developed by a low-cost hydrothermal method. The results obtained from this study indicated that Al ions could be doped successfully into the ZnO nanostructure, which could change the morphology and improve the pH-sensing properties. The pH sensitivity of Al-doped ZnO nanosheets reached 50.2 mV/pH with a correlation coefficient of around 0.99468 when compared with that of ZnO film (34.13 mV/pH) and pure ZnO nanowires (45.89 mV/pH). The test range of pH values was widened by Al-doping, and the Al-doped ZnO NS sensor could detect the pH value ranging from 2 to 12. It was observed that in a more acidic environment, especially at pH 2, the sensor, Al-doped ZnO nanosheet, was strongly stable over 12 weeks of testing. It was noted that the response time was utterly fast and the response time of the sensors for each pH standard buffer solutions was around 0.3 s. Thus, the response time and performance were quite stable. The microchannel provided a novel testing method for the pH sensor, where the liquid to be tested was just 5 mL. Hence, it was suggested to be useful for many medical diagnoses and treatments. The benefits of Al-doped ZnO nanosheet pH sensor were high sensitivity, good long-term usage, good flexible property, and requirement of a small amount of test liquid, which could make the sensors viable candidates for practical applications.

INTRODUCTION

In recent decades, pH sensors have attracted attention because of their practical application, such as medical diagnosis and treatment. A lot of research reported that the potential cancer factor had a direct relationship with the pH value of blood. It was known that the tumor cells could change the intracellular fluid to slightly acidic. This is because of the reason that for tumor cells, it was potentially easier to change glucose and other body substances into lactic acid (pH).[1] The pH value of a cancer patient's blood was usually ranging from 6.2 to 6.9 when compared with healthy people (7.3−7.4). Furthermore, the pH sensor could also be used in many biochemical monitors that could be applied in our body.[2]

Metal oxide semiconductors have been used interestingly in many research studies because of their exclusive advantages,[3] such as low cost, good integration with the microfabrication of silicon, and excellent controllability.[4] There have been a lot of studies reported on numerous pH sensors based on metal oxides, such as zinc oxide (ZnO),[5] tin(IV) oxide (SnO_2),[6] tungsten trioxide (WO_3),[7] and titanium dioxide (TiO_2).[8] Among these, ZnO has a wurtzite hexagonal structure with lattice constants of a = 0.324−0.326 nm and c = 0.513−0.543 nm, a high band gap energy (∼3.4 eV), and a high exciton binding energy (60 meV) at room temperature.[9] It was regarded as very suitable for the pH sensor because of the high crystallinity of polar and nonpolar surfaces.[10] Recently, a lot of morphology of ZnO nanostructures, such as nanowires (NWs),[11] nanorods (NRs),[12] nanotubes (NTs),[13] nanoflowers (NFs),[14] and nanosheets (NSs),[15] have been fabricated in which the microscopic sizes have been executed by varying the physical and chemical properties, and high surface-to-volume ratio. Ibupoto et al. studied the pH sensor based on

Received: August 27, 2019
Accepted: October 31, 2019
Published: November 15, 2019

DOI: 10.1021/acsomega.9b02778
ACS Omega 2019, 4, 19847−19855

immobilized ZnO NRs with lactate oxidase which showed fast response time by the hydrothermal method.[16] Maiolo et al. reported that the flexible pH sensor based on ZnO nanowalls could increase the sensitivity of pH with a higher surface-to-volume ratio.[17] Nanostructured ZnO has been fabricated by various methods, such as plasma−enhanced chemical vapor deposition,[18] microwave,[19] and hydrothermally.[20] Most of the research studies suggested that ZnO nanostructures could improve the sensitivity of the pH value, but however, ZnO nanostructures have been found to be less flexible and stable. Lee and Chiu reported that the pH sensor based on ZnO NR arrays obtained by the photo-electrochemical method could achieve a high sensitivity at 53.55, whereas it was hard to use at a lower pH value (<pH 4).[21] Therefore, it was noted that the property of the pH sensor could influence the stability, durability, and flexibility of ZnO nanostructures. Previously, a formaldehyde gas sensor based on aluminum-doped zinc oxide (AZO) thin-film with high stability and working function have been reported by Liu et al., which was fabricated with Al-doped ZnO.[22] Lin et al. also reported that AZO could enhance the stability, repeatability, and reusability for high humidity sensors.[23] The similar function was applied here due to gas sensing property, humidity detects, and pH value sensing is the chemical reaction. Thus, it was expected that the stability, durability, and flexibility of the ZnO pH sensor would be improved by aluminum doping.

The method mentioned above was applied in this work for the wider range of pH value detection, long-term use, and reusability of sensors based on Al-doped ZnO NSs. Additionally, one of the biggest drawbacks of the previously reported pH sensor was that it usually used soaking methods to detect the pH value, which could consume a large amount of solution to be tested. The miniaturization of pH sensors paid great attention on the practical application of the pH sensor, such as drinking water testing and clinical medical application. Despite the fact that a lot of successful pH sensors were already presented,[24] the research on miniaturization was still sparse. Thus, in our work, in order to deal with this issue, microfluidic technology was applied to fabricate the shrinking pH sensors, which could be portable and can test an extremely small amount of liquid sample. Kunstmann-Olsen et al. reported uniform droplet splitting and detection by microfluidic polydimethylsiloxane (PDMS).[25] In 2017, Usta et al. studied about recent advances of PDMS application to microfluidic technology,[26] and Im et al. studied the PDMS-based turbulent microfluidic mixer.[27] According to PDMS microfluidic technology, it was a good opportunity to combine with the pH sensor for miniaturization. It was reported that PDMS could not only have an easy fabrication method but also could have low cost and good binding on the glass substrate. Additionally, it was noted that a reference electrode of the pH sensor using silver−silver chloride (Ag/AgCl) ink could replace the traditional Ag/AgCl glass electrode, which could be feasibly produced very fast, and also it was easy to coat on the metal electrode.[28] The key technology of this work was that the prepared microfluidic channel could overcome the drawbacks reported by previous research studies and could also integrate the pH sensor with a microfluidic channel. On the other hand, the unique morphology was applied to fabricate the pH sensor based on Al-doped ZnO NSs with increased sensitivity and durability.

RESULTS AND DISCUSSION

Materials Characterizations. Figure 1 shows the comparison of morphology of Al-doped ZnO NSs and pure

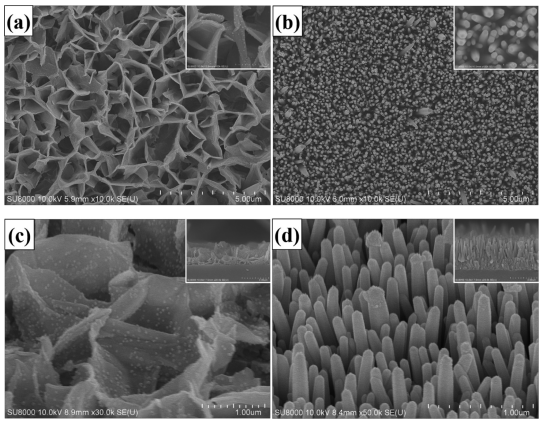

Figure 1. SEM top-view images of (a) Al-doped ZnO NSs, and (b) pure ZnO NWs. (Inset: high-resolution SEM). The SEM 45-degrees images of (c) Al-doped ZnO NSs, and (d) pure ZnO NWs. (Inset: SEM cross-section images).

ZnO NWs obtained by an ultrahigh-resolution scanning electron microscope. Figure 1a displays the scanning electron microscopy (SEM) top-view image of the Al-doped ZnO NSs, which confirmed that the NS structures were evenly distributed. The as-fabricated Al-doped ZnO NSs were constituted by several irregular high walls, with average thickness and length around 200 nm and 1 μm, respectively. Figure 1b compares the top-view image of SEM of pure ZnO NFs, which demonstrated that the synthesized ZnO NWs without Al-doping could possess the vertical, dense, and wire-like morphology, with common diameters around 80 nm. The inset of Figure 11a,b shows the high-resolution top-view image of SEM of Al-doped ZnO NSs and pure ZnO NWs, respectively, the 45° view image of SEM of Al-doped ZnO NSs and pure ZnO NWs are shown in Figure 1c,d, respectively. The inset of Figure 1c,d illustrates the SEM cross-section images of the Al-doped ZnO NSs and pure ZnO NWs, respectively. It could be seen that the average height of Al-doped ZnO NSs was 1.61 μm and that of pure ZnO NWs was 2.18 μm. It was obvious that aluminum doping could influence the morphology, density, and length of the ZnO nanostructure, and this result was similar to that of the result previously reported by Kim et al.[29]

The crystal phase of the Al-doped ZnO NSs, ZnO film, and pure ZnO NWs was measured by X-ray diffraction (XRD) as shown in Figure 2. The XRD patterns represented that the sharp diffraction peaks were in good agreement with the characteristics of the hexagonal wurtzite of ZnO (JCPDS no. 36-1451). According to previous research studies, the diffraction peaks of the Al element may not be presented in the XRD patterns, the possible reason for that could be the low doping concentration of Al, and this trend was similar to that of the result previously reported by Jantrasee.[30] Upon comparison of all the samples, the ZnO film showed the diffraction peaks centered at 2θ values of 34.4, 47.59, and 62,87° as shown in Figure 2a corresponding to the crystal planes of the hexagonal wurtzite zinc oxide (002), (102), and (103) reflections, respectively. Similar to the film, the diffraction peaks of pure ZnO NWs were observed at 34.38,

DOI: 10.1021/acsomega.9b02778
ACS Omega 2019, 4, 19847−19855

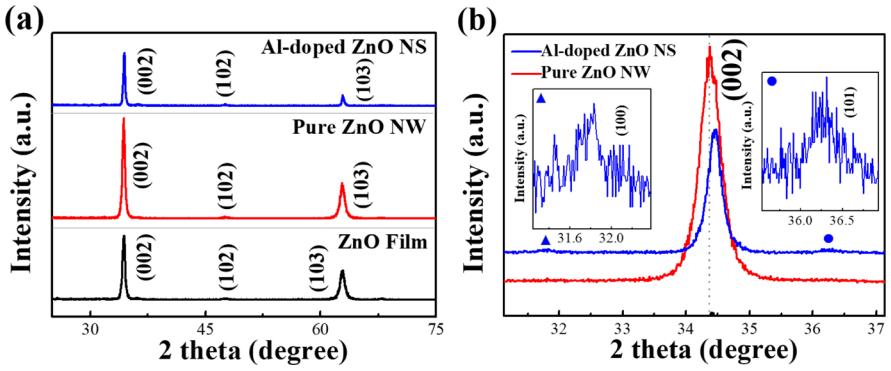

Figure 2. XRD patterns of (a) Al-doped ZnO NSs, pure ZnO NWs, and ZnO film. (b) Enlarged XRD patterns of the (002) peak.

47.54, and 62,83° corresponding to (002), (102), and (103) reflections, respectively. The Al-doped ZnO NS sample showed no diffraction peaks corresponding to the aluminum element because of the reason that the Al element was well incorporated within the ZnO lattice. The comparison of enlarged XRD patterns of the Al-doped ZnO NSs and pure ZnO NWs is shown in Figure 2b. It was found that the intensity of the (002) peak of Al-doped ZnO NSs was comparatively lower than that of pure ZnO NWs, which could reduce the surface energy of ZnO as Al replaced the Zn ions of the hexagonal wurtzite structure.[31] It was evident from the XRD pattern of Al-doped ZnO NSs that the peaks at 31.83 and 36.38° corresponded to the (100) and (101) reflections, respectively, which indicated that the Al-doping could influence the orientation of ZnO nanostructure from the *x*-axis changing to isotropic.[32] On the other hand, the (002) peak of ZnO NSs was significantly shifted to the larger diffraction angle when compared to pure ZnO NWs because of the replacement of Zn^{2+} ions (ion radius 0.74 Å) by smaller Al^{3+} ions (ion radius 0.53 Å).[33]

The crystal phase of Al-doped ZnO was further confirmed by a high-resolution transmission electron microscope as shown in Figure 3. Figure 3a shows the fragments of Al-doped ZnO NSs scraped from the sample and the inset shows the high-resolution transmission electron microscopy (HR-TEM) images. Figure 3b shows the selected area of electron diffraction (SAED) pattern, from which the lattice *d* spacing of the sample was calculated. The SAED pattern of Al-doped ZnO NSs illustrated the polycrystalline nature of the sample. The lattice *d* spacing was calculated by the following equation[34]

$$L\lambda = Rd \quad (1)$$

where *L* is the length of the camera, λ is the electron wavelength, and *R* is the radius of the ring calculated from the bright ring of the center. The SAED pattern of Al-doped ZnO NSs was calculated by eq 1, indexed as (100), (002), and (101) planes, corresponding to the polycrystalline crystallography. It was found that the Al-doped ZnO NS indexes of the SAED pattern were perfectly consistent with the XRD result. Figure 3c shows a pink rectangular frame selected area of the Al-doped ZnO NS as measured by HR-TEM elemental mapping. The sample illustrated the uniform elements of aluminum (green), zinc (red), and oxygen (yellow) element, which were consistent with the measurement of energy-dispersive X-ray (EDX) spectroscopy as shown in Figure 3d. The EDX spectrum of Al-doped ZnO NSs examined the elemental composition, which clearly illustrated that the

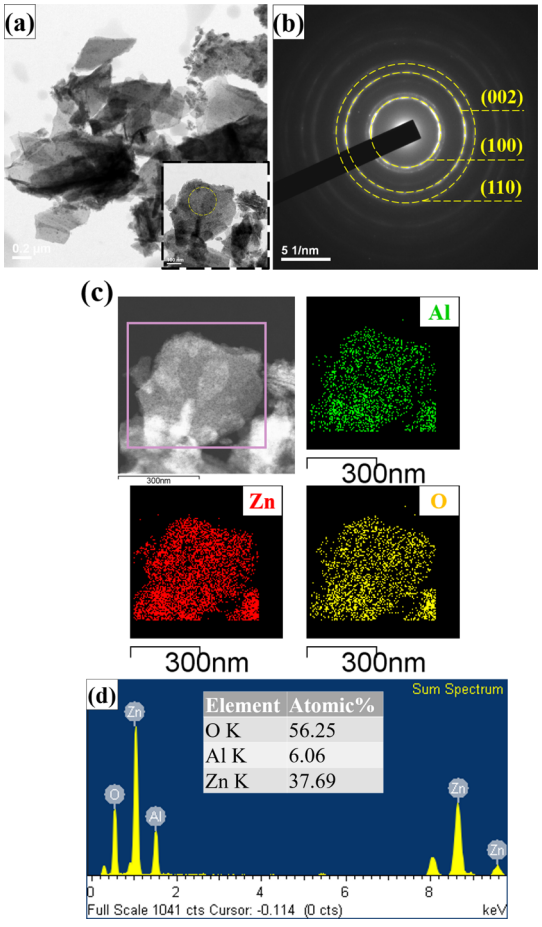

Figure 3. HR-TEM micrographs of (a) fragments of Al-doped ZnO NSs scraped from the sample (inset: high-resolution micrographs), (b) SAED pattern of Al-doped ZnO NSs, (c) elemental mapping for the selected region, revealing the presence of zinc (red), oxygen (yellow), and aluminum (green), and (d) EDX spectra of Al-doped ZnO NSs.

calculated atomic percentage of Zn, O, and Al was 37.69, 56.2, and 6.06%, respectively.

Microchannel pH Sensor Analysis and pH Value Testing. First of all, the size of the microfluidic channel of pH sensors was measured by a three dimensional (3D) measuring laser microscope (OLS5000, LEXT), and the width and height of the microchannel were around 258 and 39 μm, respectively, as shown in Figure 4.

DOI: 10.1021/acsomega.9b02778
ACS Omega 2019, 4, 19847−19855

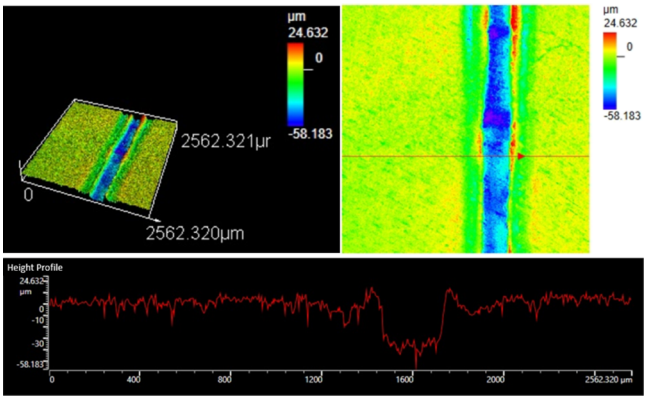

Figure 4. 3D measuring laser microscopy images of a microchannel of the pH sensor.

Figure 5 shows the pH sensitivities of the Al-doped ZnO NS pH sensor tested by an extended gate using different pH standard buffer solutions (from pH 2 to 12), and the solutions were passed through a microchannel with a reference electrode (Ag/AgCl). Figure 5a shows the source−drain current (I_{DS}) output characteristics of the pH sensor with the constant reference electrode voltage (V_G) at 3 V. It was found that the I_{DS} of the Al-doped ZnO NS pH sensor increased as the pH value of the buffer solutions decreased because of the reason that the voltage of Al-doped ZnO NSs was influenced by the acidic conditions. Accumulating H^+ ions of the solutions contributed an extra positive voltage of the sensing material, while the I_{DS} was decreased by the accumulation of OH^- ions, which corresponded to an extra negative voltage. As a result, the I_{DS} of the pH sensor could be affected by varying the pH value of the buffer solutions. Figure 8b shows the source−drain current and reference electrode voltage characteristics (I_{DS} − V_G) of the Al-doped ZnO NS pH sensor with the constant source−drain voltage (V_{DS}) at 0.2 V. It was found that the V_G was shifted to higher voltages by increasing the pH values, with relatively increased I_{DS} current from 0 A when injected into solutions with pH values ranging from 12 down to 2.

Figure 6 shows the comparison of the calculated sensitivity of the Al-doped ZnO NS, ZnO NW, and ZnO film sensor. The relationship between the I_{DS} and pH value of sensors could be assessed by basic metal-oxide-semiconductor field-effect transistors,[35] where the altered threshold voltage (V_T) depended on pH value. The saturation region was defined by the following equation[36]

$$I_{DS} = \frac{1}{2}K_n[(V_{GS} - V_T)^2] \quad (2)$$

and for the linear region

$$I_{DS} = \frac{1}{2}K_n\left[(V_{GS} - V_T) - \frac{1}{2}V_{DS}\right] \quad (3)$$

where K_n is the conduction parameter, V_{GS} is the source−gate voltage that is related to the V_G, and V_{DS} is the drain−source voltage. The dependence of V_T on pH was presented by Chou et al.[37] Figure 6a represents the three-round testing sensitivity of the ZnO thin film, which was found to be 34.13, 32.21, and 33.48 mV/pH with correlation coefficients of 0.99233, 0.9828, and 0.9815, respectively. Figure 6b shows the three-round pH sensitivity measurements of the ZnO NW which was found to be 44.54, 45.35, and 45.89 mV/pH with correlation coefficients of 0.99204, 0.99191, and 0.9919, respectively. Figure 6c shows the sensitivity of Al-doped ZnO NSs by three-round testing results which was found to be 49.62, 48.19, and 50.3 mV/pH with correlation coefficients of 0.99742, 0.99229, and 0.99468, respectively. It was found that the ZnO NW could increase the sensitivity of the pH value, whereas the stability and flexibility decreased. However, it was observed that it could not sense the pH 2 solution. According to previous studies, ZnO NWs can improve sensing performance because of a large sensing surface-to-volume ratio, while the surface-to-volume ratio leads the material to come in contact with many buffer solutions. Also, zinc oxide is a material that is relatively easy to react with the acidic solution; as a result, the ZnO NW pH sensor is destroyed when pH 2 solution is tested, and this result is quite similar with the previous research.[38] The sensitivity of Al-doped ZnO NSs was also improved and was higher than that of ZnO NWs, and thus, it displayed better stability and flexibility over the pH ranging from pH 2 to pH 12. Actually Al-doping caused the ZnO nanostructure to be more flexible and stable.[39] In addition, all the three-round testing sensitivities of the pH value of each sensor almost showed the same results, where the potential changes of the sensors were affected very little by testing several pH levels. According to the previous reports, it was reported that once the potential deviation of sensors was less than ±5 mV, the applications of sensors would be valuable and reliable.[40]

The response time of the pH sensor with a microchannel was tested by the buffer solutions from pH 2 to pH 12 as shown in Figure 7. According to the previous reports, the response time of pH sensors could be commonly defined as the time of 90% of the sensors reaching a stable potential.[41] Figure 7 shows the response time of the Al-doped ZnO NS pH sensor

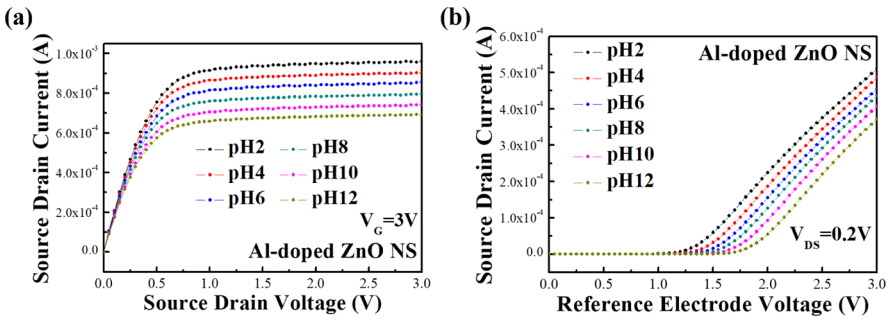

Figure 5. (a) Drain−source current and drain−source voltage characteristics, and (b) drain−source current and reference electrode voltage characteristics of the Al-doped ZnO NS pH sensor with the microchannel.

DOI: 10.1021/acsomega.9b02778
ACS Omega 2019, 4, 19847−19855

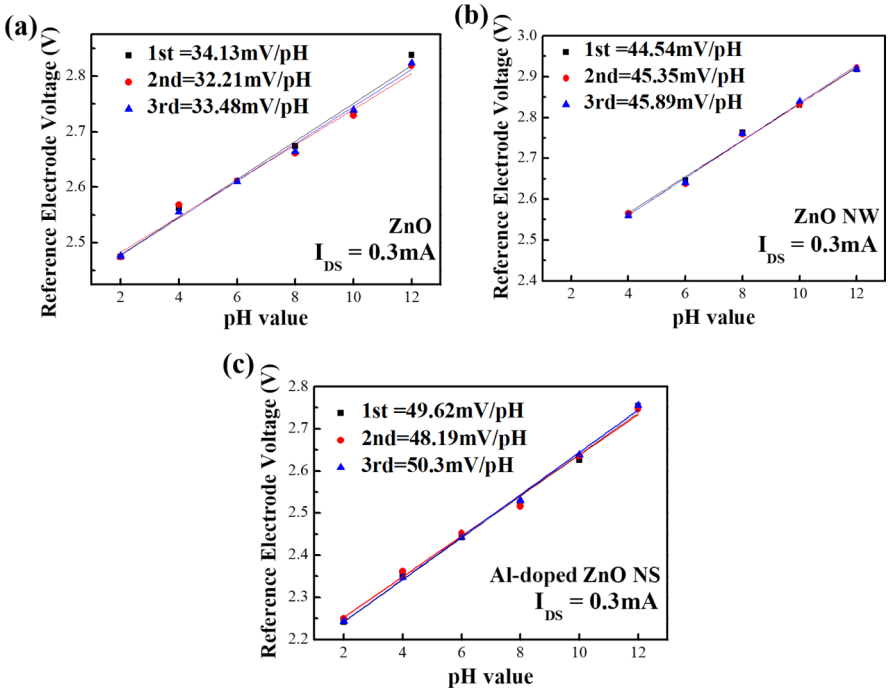

Figure 6. Three-rounds pH responses of (a) ZnO film, (b) ZnO NWs, (c) Al-doped ZnO NSs from pH 2 to pH 12.

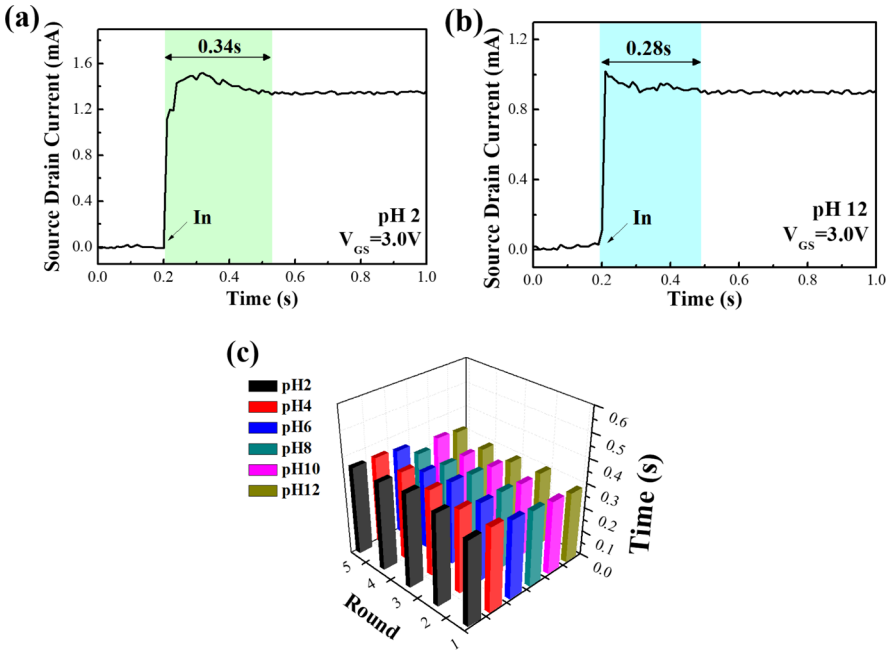

Figure 7. pH responses of Al-doped ZnO NSs in terms of response time in several buffer solutions with (a) pH 2 value, (b) pH 12 value, and (c) statistic chart from pH 2 to pH 12.

with the microchannel at pH 2 and pH 12. In the beginning, the current of sensors remain stable at zero, after 0.2 s the pH solutions are injected to the sensors and the sensors' reactions become stable at around 0.5 s. The total reaction time takes around 0.3 s from the time of injection (0.2 s) to the chemical reactions becoming stable (around 0.5 s). The time from the injection to reach the stable potential was found to be 0.34 s for pH 2 and 0.28 s for pH 12, where the pH sensors tested with a microchannel were extremely faster than the soaking method. The statistical analysis of the response time is shown in Figure 7c. It was observed that the response time of the pH sensor with a microchannel was found to be 0.3 s for any pH value, all with the same value for five rounds of testing in each pH which was very stable and quick. The response time and reliability of pH sensors were necessary for many applications such as biochemical monitors.

Figure 8 compares the durability of ZnO film and Al-doped ZnO NSs for a duration of 12 weeks. The source−drain current output characteristics of ZnO film and Al-doped ZnO NSs in pH 2 was between 0 and 12 weeks. It was found that the ZnO NW could not response at pH 2 because of a more acidic environment, and the ZnO film would be unstable after

DOI: 10.1021/acsomega.9b02778
ACS Omega 2019, 4, 19847−19855

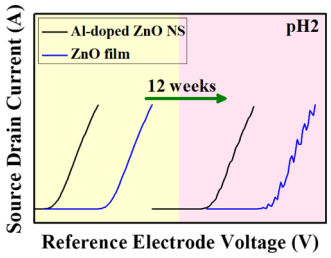

Figure 8. Comparison of the durability of ZnO film and Al-doped ZnO NSs in terms of 12 weeks in pH 2.

12 weeks; however, Al-doped ZnO NSs exhibited enhanced stability and durability properties after 12 weeks. Thus, it was suggested that both the reliability and long-term usage of pH sensors should be considered for the applications.

Mechanism of Al-Doped ZnO NS pH-Testing. Basically, the surface of metal oxides was hydrolyzed by water and thus hydroxide was formed on the surface. The surface would become rich in the polar hydroxyl (−OH) groups as the polar water molecules were adsorbed by the layer physically. Once the Al-doped ZnO NS has undergone a chemical reaction with an electrolyte, the surface charge would be increased by several reasons such as adsorption of ions, accumulation or consumption of the surface charge from the surface of materials, and physical adsorption of surface charge. The H-specific binding sites of the material would be hydrogenated when the surface of Al-doped ZnO NSs was in contact with the buffer solution, which could protonate or deprotonate the binding sites of the material because of the increase or decrease of the surface charge at different pH values of the solutions.[42] In addition, the Al-doped ZnO NS could chemically react with acidic and basic solutions because the material was an amphoteric oxide. The chemical reaction of acidic and basic solutions could be defined by the following eqs 4 and 5, respectively.

In acid buffer

$$ZnO + 2OH^- + H_2O \rightarrow Zn(OH)_4^{2-} \quad (4)$$

In basic buffer

$$ZnO + 2H_3O^+ + 3H_2O \rightarrow Zn(H_2O)_6^{+} \quad (5)$$

pH-sensing tests of ZnO film, ZnO NWs, and Al-doped ZnO NSs were divided into two probable ways for the pH values of solutions such as <pH 7 and >pH 7. In the acidic buffer, the potential difference of the solutions was found to be higher than the materials, where the solutions contained more H^+ compared with the binding sites of the materials. By contrast, in the basic buffer, the charged surface of the materials would lose protons to form OH^-, where the surface of materials would become negatively charged.[43] The pH-sensing property of Al-doped ZnO NSs might be attributed for several reasons. First, the morphology effect, that is, the surface to volume ratio of Al-doped ZnO NSs was much higher than that of the others. The possible mechanism proposed for pH-sensing of Al-doped ZnO NSs is shown in Figure 9. In the present work, Al doping caused a change in the morphology of ZnO nanostructures, as shown in the SEM images (Figure 1). As we mentioned above, the pH-sensing chemical reaction occurred when the electrolyte solution was in contact with the surface of the metal oxides. Thus, the responses of pH sensors increased with the increase of the surface to volume ratio. Second, the oxygen vacancies of Al-doped ZnO NSs should also produce considerable effects on the pH-sensing properties because the oxygen vacancies could influence the number of binding sites for the pH-sensing reaction. In our previous study, based on the EDX spectra it was reported that the Al-doped ZnO NS possessed more oxygen vacancies,[15] as shown in Figure 3d. Upon the formation of unsaturated dangling bonds at the surface, the surface would produce more oxygen vacancies, which could lead the fast chemical reaction. Thus, the ability of chemical adsorption and desorption with the surface would increase.[44] Table 1 shows the comparison of the pH-sensing property of pH sensors based on several metal oxide materials with the pH sensors reported in previous studies. It was thus suggested that the microfluidic Al-doped ZnO NS pH sensor possessed good sensitivity, extremely fast response time, flexibility, long-term utility, and reliability. Also, the pH testing solutions are just needed a few due to microfluidic integrate with the pH sensor.

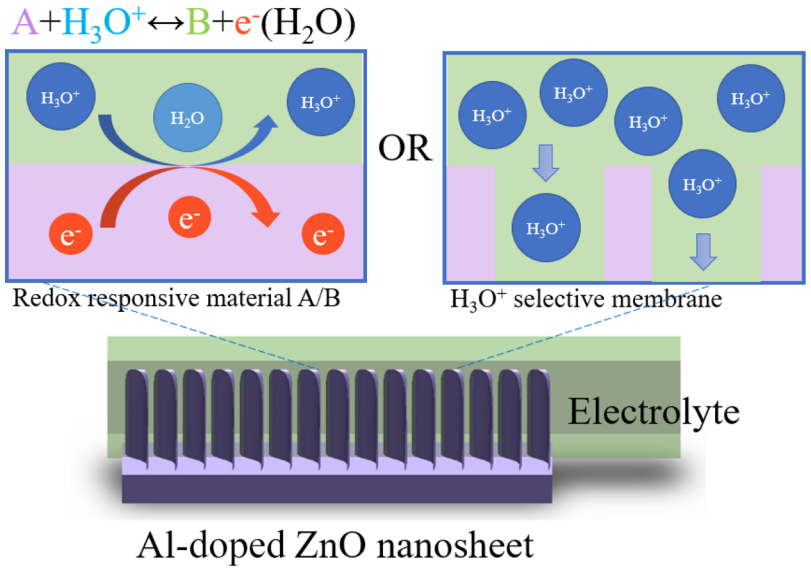

Figure 9. Schematic representation of possible sensing mechanisms of the Al-doped ZnO NS pH sensor.

DOI: 10.1021/acsomega.9b02778
ACS Omega 2019, 4, 19847−19855

Table 1. Comparison of the Properties of Pure ZnO NWs and Al-Doped ZnO NS pH Sensors with the Previous Reports

sensor materials	pH range	sensitivity (mV/pH)	response time (s)	electrolyte volume	references
ZnO thin film	2−12	38		immersed in electrolyte	36
ZnO NTs/NRs	4−12	45.9		immersed in electrolyte	47
TiO_2 NW	4−10	32.65		immersed in electrolyte	48
SnO_2 thin film	2−10	39		immersed in electrolyte	49
silicon NWs	1−11	58.3		immersed in electrolyte	50
ZnO/Ta thin film	1.3−12	41.56		immersed in electrolyte	51
InGaZnO thin film	3−10	59.2	<300	immersed in electrolyte	52
ZnO thin film	2−9	43.71	29	5 mL	53
ZnO NW	4−12	45.89	<0.5	5 mL	present work
Al-doped ZnO NW	2−12	50.3	<0.5	5 mL	

CONCLUSIONS

In conclusion, we have demonstrated a microfluidic pH sensor with the novel morphology of ZnO nanostructures based on Al-doped ZnO NSs by the hydrothermal method and the sensor showed flexible, reliable, high response, and fast response time. The results illustrated that the pH sensitivities increased from 34.13 mV/pH (ZnO film) to 50.3 mV/pH (Al-doped ZnO NS) and the sensitivities were very stable for three-round testing. The pH-sensing response time was found to be around 0.3 s, which was extremely fast. The flexible property of Al-doped ZnO NSs was also improved, over the pH ranging from pH 2 to pH 12 and upon long-term use, and the sensor still remained stable after 12 weeks testing. A new detection method was thus provided by the microchannel, where the testing solution required was just 5 mL only. This study might provide a significant potential of pH sensors for the applications in many biochemical monitors that could be applied in our body.

EXPERIMENTAL SECTION

Fabrication of Al-Doped ZnO NSs and pH Sensors. The Al-doped ZnO NSs were fabricated in two stages: first, 50 nm Al film as a seed layer was evaporated on a glass substrate by electron beam evaporation. Second, a low-temperature hydrothermal process was carried out using zinc nitrate hydrate $[Zn(NO_3)_2{\cdot}6H_2O]$ and hexamethylenetetramine ($C_6H_{12}N_4$, HMTA). To fabricate the Al-doped ZnO NSs, aqueous solution of 60 mM zinc nitrate and 60 mM HMTA were mixed into deionized water (DI water), and then stirred for 15 min at 90 °C.[45] The prepared solution and the substrate were transferred into a serum bottle and heated at 95 °C for 1 h. After the reaction was completed, the serum bottle was cooled to room temperature, then the glass substrate was washed with acetone and DI water, and dried in air. The properties of three varieties of pH sensors such as: (1) ZnO film, (2) ZnO NW, and (3) ZnO NS were compared. Figure 10 shows a schematic representation and picture of the Al-doped ZnO NS structured pH sensor. First, the glass substrate was washed with acetone, isopropanol, and DI water with an ultrasonic cleaner for 15 min. Then, the platinum (Pt) working and reference electrodes were evaporated by electron beam evaporation. The chamber was evacuated down to 5×10^6 Torr and kept the voltage and current of the electron gun over 4.5 kV and 15 mA, respectively, and platinum vapor was continuously deposited on the substrate until the thickness was reached up to 100 nm. A definite region of the synthesized sensing film was controlled by photoresist. The three different sensing structures were obtained for the working electrode as mentioned above with a region of 1 cm × 250 μm. The inset of Figure 10 shows the SEM image of Al-doped ZnO NSs. The thickness of Ag/AgCl ink (cat#011464, ALS Co., Ltd., Japan) was approximately 150 μm with a region of 1 cm × 250 μm as a reference electrode, which was fabricated on the Pt electrode by using a hot plate at 95 °C for 30 min.

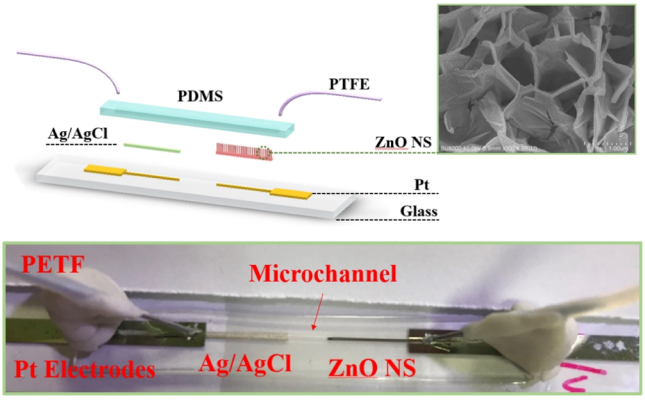

Figure 10. Schematic cartoon image and photograph of the pH sensor of the Al-doped ZnO NS with the microchannel.

Microfluidic System Development and Measurement System Setup. Figure 11 shows the fabrication process of a microchannel in PDMS combined with the pH sensor. The main fabrication of PDMS layer using traditional photolithography technology and expansion of formerly presented researches.[46] The layout for masks was drawn by a computer-aided design program (AutoCAD 2011, Autodesk, the United States). A master formed on a silicon wafer using a negative-tone UV photoresist (SU8-2100, MicroChem Corporation, Newton, MA), which has thin flat layers with a microchannel was fabricated. A curing agent and PDMS (cat#SYGARD-184AB, Goal Bio, R. O. C.) at a 1:10 weight ratio were completely stirred. Then, this mixture was degassed by a mechanical vacuum pump at 30 mTorr for 1 h, which could remove any air bubbles and make sure the mixing was uniform. The prepolymer mixture was poured onto the master mold, and then it was cured for 4 h at 100 °C in an oven. After curing, PDMS was peeled off from the master mold and then bonded to the pH sensor by oxygen plasma bonding. The width, height, and length of the microchannel were 250 μm, 35 μm, and 3 cm, respectively. Finally, a polytetrafluoroethylene tube with a needle was attached to both sides of the microchannel and fixed with adhesive and clay.

Figure 12 shows the measuring system of the microfluidic pH sensor. The sensing region was connected to the gate of a commercial metal-oxide-semiconductor field-effect transistor (MOSFET, CD4007UB). The pH sensor was measured by the Agilent B2902A Precision source/measure unit with pH standard buffer solution varied from 2 to 12 ± 0.02 (GREAT and BEST Co., Ltd, R. O. C.). The property of pH sensors was defined by the potentiometric method, which

DOI: 10.1021/acsomega.9b02778
ACS Omega 2019, 4, 19847−19855

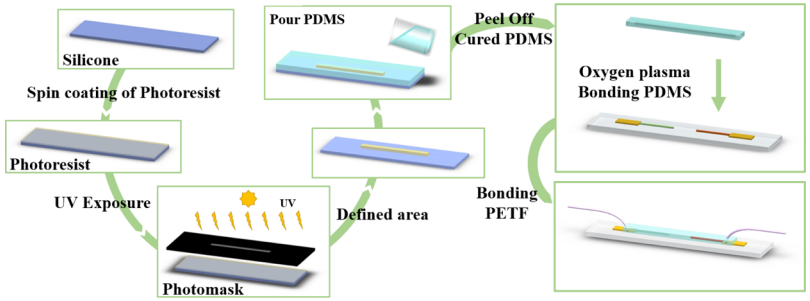

Figure 11. Schematic graphs showing the fabricating process of microfluidic PDMS and bonding to the pH sensor.

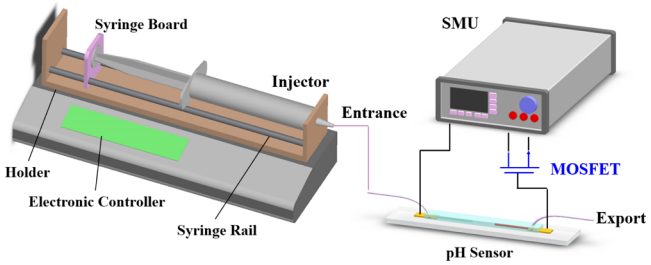

Figure 12. Schematic representation of the experimental measurement system setup and pH sensor testing.

was calculated from the potential difference between the reference electrode (Ag/AgCl) and the sensing electrode. First of all, the pH standard buffer solution was inspected by a pH meter. (F-51, HORIBA, Ltd., Japan), then the buffer solution was injected into our pH sensor by a syringe pump. After injection, the microchannel was washed with ethanol and DI water at each testing. The pH sensor with microfluidic was measured by the buffer solution from alkaline (pH 12) to acidic (pH 2) for sensitivity, durability, stability, and repeatability.

Characterization. The morphology of Al-doped ZnO NSs, pure ZnO NWs, and ZnO films were characterized by an ultrahigh-resolution scanning electron microscope (Hitachi SU8000, Japan), and analyzed by XRD (18 kW Rotating Anode X-ray Generator, Rigaku). The Al-doped ZnO NSs were measured by a high-resolution transmission electron microscope and energy dispersive spectrometer (JEOL JEM-2100F CS-STEM, Japan).

AUTHOR INFORMATION

Corresponding Author

*E-mail: lwji@seed.net.tw.

ORCID

You-Ting Tsai: 0000-0002-0709-4463

Liang-Wen Ji: 0000-0003-2475-0589

Notes

The authors declare no competing financial interest.

REFERENCES

(1) Damaghi, M.; Wojtkowiak, J. W.; Gillies, R. J. pH sensing and regulation in cancer. *Front. Physiol.* **2013**, *4*, 370.

(2) Liu, J.; Huang, Y.; Kumar, A.; Tan, A.; Jin, S.; Mozhi, A.; Liang, X.-J. pH-sensitive nano-systems for drug delivery in cancer therapy. *Adv. Biotech.* **2014**, *32*, 693−710.

(3) Schultealbert, C.; Baur, T.; Schütze, A.; Böttcher, S.; Sauerwald, T. A novel approach towards calibrated measurement of trace gases using metal oxide semiconductor sensors. *Sens. Actuators, B* **2017**, *239*, 390−396.

(4) Grundmann, M.. Transparent Conductive Oxide Semiconductors. *The Physics of Semiconductors*; Springer, 2016; pp 575−579.

(5) Li, H.-H.; Yang, C.-E.; Kei, C.-C.; Su, C.-Y.; Dai, W.-S.; Tseng, J.-K.; Yang, P.-Y.; Chou, J.-C.; Cheng, H.-C. Coaxial-structured ZnO/silicon nanowires extended-gate field-effect transistor as pH sensor. *Thin Solid Films* **2013**, *529*, 173−176.

(6) Chin, Y.-L.; Chou, J.-C.; Sun, T.-P.; Liao, H.-K.; Chung, W.-Y.; Hsiung, S.-K. A novel SnO_2/Al discrete gate ISFET pH sensor with CMOS standard process. *Sens. Actuators, B* **2001**, *75*, 36−42.

(7) Santos, L.; Neto, J. P.; Crespo, A.; Nunes, D.; Costa, N.; Fonseca, I. M.; Barquinha, P.; Pereira, L.; Silva, J.; Martins, R.; Fortunato, E. WO_3 nanoparticle-based conformable pH sensor. *ACS Appl. Mater. Interfaces* **2014**, *6*, 12226−12234.

(8) Zhao, R.; Xu, M.; Wang, J.; Chen, G. A pH sensor based on the TiO_2 nanotube array modified Ti electrode. *Electrochim. Acta* **2010**, *55*, 5647−5651.

(9) Katwal, G.; Paulose, M.; Rusakova, I. A.; Martinez, J. E.; Varghese, O. K. Rapid growth of zinc oxide nanotube-nanowire hybrid architectures and their use in breast cancer-related volatile organics detection. *Nano Lett.* **2016**, *16*, 3014−3021.

(10) Lokesh, K.; Kavitha, G.; Manikandan, E.; Mani, G. K.; Kaviyarasu, K.; Rayappan, J. B. B.; Ladchumananandasivam, R.; Sundeep Aanand, J.; Jayachandran, M.; Maaza, M. Effective ammonia detection using n-ZnO/p-NiO heterostructured nanofibers. *IEEE Sens. J.* **2016**, *16*, 2477−2483.

(11) Malakooti, M. H.; Patterson, B. A.; Hwang, H.-S.; Sodano, H. A. ZnO nanowire interfaces for high strength multifunctional composites with embedded energy harvesting. *Energy Environ. Sci.* **2016**, *9*, 634−643.

(12) Bagchi, D.; Maji, T. K.; Sardar, S.; Lemmens, P.; Bhattacharya, C.; Karmakar, D.; Pal, S. K. Sensitized ZnO nanorod assemblies to detect heavy metal contaminated phytomedicines: spectroscopic and simulation studies. *Phys. Chem. Chem. Phys.* **2017**, *19*, 2503−2513.

(13) Roza, L.; Rahman, M. Y. A.; Umar, A. A.; Salleh, M. M. Direct growth of oriented ZnO nanotubes by self-selective etching at lower temperature for photo-electrochemical (PEC) solar cell application. *J. Alloys Compd.* **2015**, *618*, 153−158.

(14) Tsai, Y.-T.; Chang, S.-J.; Ji, L.-W.; Hsiao, Y.-J.; Tang, I.-T.; Lu, H.-Y.; Chu, Y.-L. High Sensitivity of NO Gas Sensors Based on Novel Ag-Doped ZnO Nanoflowers Enhanced with a UV Light-Emitting Diode. *ACS Omega* **2018**, *3*, 13798−13807.

(15) Tsai, Y.-T.; Chang, S.-J.; Tang, I.-T.; Hsiao, Y.-J.; Ji, L.-W. High density novel porous ZnO nanosheets based on a microheater chip for ozone sensors. *IEEE Sens. J.* **2018**, *18*, 5559−5565.

(16) Ibupoto, Z. H.; Shah, S. M. U. A.; Khun, K.; Willander, M. Electrochemical L-lactic acid sensor based on immobilized ZnO nanorods with lactate oxidase. *Sensors* **2012**, *12*, 2456−2466.

(17) Maiolo, L.; Mirabella, S.; Maita, F.; Alberti, A.; Minotti, A.; Strano, V.; Pecora, A.; Shacham-Diamand, Y.; Fortunato, G. Flexible pH sensors based on polysilicon thin film transistors and ZnO nanowalls. *Appl. Phys. Lett.* **2014**, *105*, 093501.

(18) Barreca, D.; Bekermann, D.; Comini, E.; Devi, A.; Fischer, R. A.; Gasparotto, A.; Maccato, C.; Sberveglieri, G.; Tondello, E. 1D

DOI: 10.1021/acsomega.9b02778
ACS Omega 2019, 4, 19847−19855

ZnO nano-assemblies by Plasma-CVD as chemical sensors for flammable and toxic gases. *Sens. Actuators, B* **2010**, *149*, 1−7.
(19) Chen, Y. J.; Cao, M. S.; Wang, T. H.; Wan, Q. Microwave absorption properties of the ZnO nanowire-polyester composites. *Appl. Phys. Lett.* **2004**, *84*, 3367−3369.
(20) Sinha, M.; Mahapatra, R.; Mondal, B.; Maruyama, T.; Ghosh, R. Ultrafast and reversible gas-sensing properties of ZnO nanowire arrays grown by hydrothermal technique. *J. Phys. Chem. C* **2016**, *120*, 3019−3025.
(21) Lee, C.-T.; Chiu, Y.-S. Photoelectrochemical passivated ZnO-based nanorod structured glucose biosensors using gate-recessed AlGaN/GaN ion-sensitive field-effect-transistors. *Sens. Actuators, B* **2015**, *210*, 756−761.
(22) Chi, C.-Y.; Chen, H.-I.; Chen, W.-C.; Chang, C.-H.; Liu, W.-C. Formaldehyde sensing characteristics of an aluminum-doped zinc oxide (AZO) thin-film-based sensor. *Sens. Actuators, B* **2018**, *255*, 3017−3024.
(23) Lee, C.-H.; Chuang, W.-Y.; Lin, S.-H.; Wu, W.-J.; Lin, C.-T. A printable humidity sensing material based on conductive polymer and nanoparticles composites. *Jpn. J. Appl. Phys.* **2013**, *52*, 05DA08.
(24) Scandurra, A.; Bruno, E.; Condorelli, G. G.; Grimaldi, M. G.; Mirabella, S. Microscopic model for pH sensing mechanism in zinc-based nanowalls. *Sens. Actuators, B* **2019**, *296*, 126614.
(25) Kunstmann-Olsen, C.; Hanczyc, M. M.; Hoyland, J.; Rasmussen, S.; Rubahn, H.-G. Uniform droplet splitting and detection using Lab-on-Chip flow cytometry on a microfluidic PDMS device. *Sens. Actuators, B* **2016**, *229*, 7−13.
(26) Gokaltun, A.; Yarmush, M. L.; Asatekin, A.; Usta, O. B. Recent advances in nonbiofouling PDMS surface modification strategies applicable to microfluidic technology. *Technology* **2017**, *05*, 1−12.
(27) You, J. B.; Kang, K.; Tran, T. T.; Park, H.; Hwang, W. R.; Kim, J. M.; Im, S. G. PDMS-based turbulent microfluidic mixer. *Lab Chip* **2015**, *15*, 1727−1735.
(28) Shitanda, I.; Kiryu, H.; Itagaki, M. Improvement in the long-term stability of screen-printed planar type solid-state Ag/AgCl reference electrode by introducing poly (dimethylsiloxane) liquid junction. *Electrochim. Acta* **2011**, *58*, 528−531.
(29) Kim, K.-H.; Kumar, B.; Lee, K. Y.; Park, H. K.; Lee, J. H.; Lee, H. H.; Jun, H.; Lee, D.; Kim, S. W. Piezoelectric two-dimensional nanosheets/anionic layer heterojunction for efficient direct current power generation. *Sci. Rep.* **2013**, *3*, 2017.
(30) Jantrasee, S.; Moontragoon, P.; Pinitsoontorn, S. Thermo-electric properties of Al-doped ZnO: experiment and simulation. *J. Semicond.* **2016**, *37*, 092002.
(31) Manoharan, C.; Pavithra, G.; Bououdina, M.; Dhanapandian, S.; Dhamodharan, P. Characterization and study of antibacterial activity of spray pyrolysed ZnO: Al thin films. *Appl. Nanosci.* **2016**, *6*, 815−825.
(32) Zi-qiang, X.; Hong, D.; Yan, L.; Hang, C. Al-doping effects on structure, electrical and optical properties of c-axis-orientated ZnO: Al thin films. *Mater. Sci. Semicond. Process.* **2006**, *9*, 132−135.
(33) Hou, Q.; Meng, F.; Sun, J. Electrical and optical properties of Al-doped ZnO and $ZnAl_2O_4$ films prepared by atomic layer deposition. *Nanoscale Res. Lett.* **2013**, *8*, 144.
(34) Kaur, G.; Mitra, A.; Yadav, K. L. Pulsed laser deposited Al-doped ZnO thin films for optical applications. *Prog. Nat. Sci.* **2015**, *25*, 12−21.
(35) Taur, Y.; Lin, H. H. Modeling of DG MOSFET I-V Characteristics in the Saturation Region. *IEEE Trans. Electron Devices* **2018**, *65*, 1714−1720.
(36) Batista, P.; Mulato, M. ZnO extended-gate field-effect transistors as pH sensors. *Appl. Phys. Lett.* **2005**, *87*, 143508.
(37) Chiang, J. L.; Chen, Y. C.; Chou, J. C. Simulation and experimental study of the pH-sensing property for AlN thin films. *Jpn. J. Appl. Phys.* **2001**, *40*, 5900.
(38) Chang, S.-P.; Li, C.-W.; Chen, K.-J.; Chang, S.-J.; Hsu, C.-L.; Hsueh, T.-J.; Hsueh, H.-T. ZnO-nanowire-based extended-gate field-effect-transistor pH sensors prepared on glass substrate. *Sci. Adv. Mater.* **2012**, *4*, 1174−1178.
(39) Hao, X.; Ma, J.; Zhang, D.; Yang, T.; Ma, H.; Yang, Y.; Cheng, C.; Huang, J. Thickness dependence of structural, optical and electrical properties of ZnO: Al films prepared on flexible substrates. *Appl. Surf. Sci.* **2001**, *183*, 137−142.
(40) Huang, W.-D.; Cao, H.; Deb, S.; Chiao, M.; Chiao, J. C. A flexible pH sensor based on the iridium oxide sensing film. *Sens. Actuators, A* **2011**, *169*, 1−11.
(41) Yao, S.; Wang, M.; Madou, M. A pH electrode based on melt-oxidized iridium oxide. *J. Electrochem. Soc.* **2001**, *148*, H29−H36.
(42) Ali, S. M. U.; Nur, O.; Willander, M.; Danielsson, B. A fast and sensitive potentiometric glucose microsensor based on glucose oxidase coated ZnO nanowires grown on a thin silver wire. *Sens. Actuators, B* **2010**, *145*, 869−874.
(43) Haarindraprasad, R.; Hashim, U.; Gopinath, S. C. B.; Kashif, M.; Veeradasan, P.; Balakrishnan, S. R.; Foo, K. L.; Poopalan, P. Low temperature annealed zinc oxide nanostructured thin film-based transducers: characterization for sensing applications. *PLoS One* **2015**, *10*, No. e0132755.
(44) Meng, F.; Hou, N.; Ge, S.; Sun, B.; Jin, Z.; Shen, W.; Kong, L.; Guo, Z.; Sun, Y.; Wu, H. , Flower-like hierarchical structures consisting of porous single-crystalline ZnO nanosheets and their gas sensing properties to volatile organic compounds (VOCs). *J. Alloys Compd.* **2015**, *626*, 124−130.
(45) Baruah, S.; Dutta, J. Hydrothermal growth of ZnO nanostructures. *Sci. Techmol. Adv. Mat.* **2009**, *10*, 013001.
(46) Cong, H.; Pan, T. Photopatternable conductive PDMS materials for microfabrication. *Adv. Funct. Mater.* **2008**, *18*, 1912−1921.
(47) Fulati, A.; Usman Ali, S.; Riaz, M.; Amin, G.; Nur, O.; Willander, M. Miniaturized pH sensors based on zinc oxide nanotubes/nanorods. *Sensors* **2009**, *9*, 8911−8923.
(48) Li, J.-Y.; Chang, S.-P.; Chang, S.-J.; Tsai, T.-Y. Sensitivity of EGFET pH sensors with TiO_2 nanowires. *ECS Solid State Lett.* **2014**, *3*, P123−P126.
(49) Batista, P. D.; Mulato, M.; Graeff, C. F. d. O.; Fernandez, F. J. R.; Marques, F. d. C. SnO_2 extended gate field-effect transistor as pH sensor. *Braz. J. Phys.* **2006**, *36*, 478−481.
(50) Hsu, J.-F.; Huang, B.-R.; Huang, C.-S.; Chen, H.-L. Silicon nanowires as pH sensor. *Jpn. J. Appl. Phys.* **2005**, *44*, 2626.
(51) Chiu, Y.-S.; Lee, C.-T.; Lou, L.-R.; Ho, S.-C.; Chuang, C.-T. Wide linear sensing sensors using ZnO: Ta extended-gate field-effect-transistors. *Sens. Actuators, B* **2013**, *188*, 944−948.
(52) Jang, H.-J.; Gu, J.-G.; Cho, W.-J. Sensitivity enhancement of amorphous InGaZnO thin film transistor based extended gate field-effect transistors with dual-gate operation. *Sens. Actuators, B* **2013**, *181*, 880−884.
(53) Mani, G. K.; Morohoshi, M.; Yasoda, Y.; Yokoyama, S.; Kimura, H.; Tsuchiya, K. ZnO-based microfluidic pH sensor: a versatile approach for quick recognition of circulating tumor cells in blood. *ACS Appl. Mater. Interfaces* **2017**, *9*, 5193−5203.

DOI: 10.1021/acsomega.9b02778
ACS Omega 2019, 4, 19847−19855